J|A|C|S COMMUNICATIONS

Published on Web 03/24/2010

Truncated Octahedral Pt_3Ni Oxygen Reduction Reaction Electrocatalysts

Jianbo Wu,[†] Junliang Zhang,[‡] Zhenmeng Peng,[†] Shengchun Yang,[†] Frederick T. Wagner,[‡] and Hong Yang*,[†]

Department of Chemical Engineering, University of Rochester, Gavett Hall 206, Rochester, New York 14627, and Electrochemical Energy Research Lab, General Motors Research and Development, Honeoye Falls, New York 14472

Received January 21, 2010; E-mail: hongyang@che.rochester.edu

Improving the sluggish kinetics of the electrocatalytic oxygen reduction reaction (ORR) is critical to advancing hydrogen fuel cell technology.[1] An important threshold value in ORR catalyst activity is a 4-fold improvement in activity per unit mass of Pt over the current commercial carbon-supported Pt (Pt/C) catalysts that are used in vehicle fuel cells to allow fuel-cell power trains to become cost-competitive with their internal-combustion counterparts.[1a,b] While great advancements have been made in recent years, the Pt area-specific ORR activity of the best catalysts is still far below the value that has been demonstrated for the Pt_3Ni (111) single-crystal surface, which is 90 times that of Pt/C.[2] A 9-fold enhancement in area-specific activity has been achieved by changing from the (100) to the (111) Pt_3Ni crystal surface. This result is very intriguing and is an important clue for the development of next-generation ORR catalysts.[2−5] In the past several years, substantial research efforts have been directed toward shape and composition controls of Pt binary metal nanoparticles to meet the challenges in the preparation of highly active catalysts.[6] While size, shape, and composition must be tightly controlled in order to have the proper surface atomic arrangement and electronic properties, it is also the case that the conventional thermal treatment cannot be readily applied to treat the Pt nanoparticles to effectively remove the surface capping agents that are typically required for producing nanocrystals, as the temperature range used is often too high to preserve the morphologies. Without removal of the surface molecules, active catalytic sites are often blocked.

In this paper, we present a facile approach to the preparation of truncated-octahedral Pt_3Ni (*t,o*-Pt_3Ni) catalysts that have dominant exposure of {111} facets. While thermally annealed alloy catalysts typically take on cuboctahedral or truncated-octahedral shapes, greater uniformity of shape and higher levels of crystalline and compositional control within each facet can be expected for shape-controlled nanocrystals. Butylamine is used in the room-temperature surface treatment to replace the capping agents used in the synthesis of *t,o*-Pt_3Ni nanocrystals and to create carbon-supported and shape-defined active electrocatalysts.

The shape-defined Pt−Ni nanoparticles were made from platinum acetylacetonate [$Pt(acac)_2$] and nickel acetylacetonate [$Ni(acac)_2$] in diphenyl ether (DPE) using a mixture of borane-*tert*-butylamine complex (TBAB) and hexadecanediol as the reducing agents (see the Supporting Information). Long-alkane-chain amines were used as the main capping agent, and adamantanecarboxylic acid (ACA) or adamantaneacetic acid (AAA) was used to affect the reaction kinetics, which is important in determining the shape of the nanocrystals.[7] Figure 1 shows transmission electron microscopy (TEM) images of cubic and truncated-octahedral nanocrystals made under three different sets of conditions. The population of truncated octahedra depended on the types and amounts of reducing and capping agents used. Among the various capping agents, short-alkane-chain amines appeared to favor the formation of {111} facets. The highest population of cubes was observed when octadecylamine was used (Figure S1 in the Supporting Information), and a small portion of cubes could still be observed when hexadecylamine was chosen (Figure 1a,b). Only octahedra and truncated octahedra were formed when dodecylamine was used (Figure 1c). The *d* spacing of the lattice was 0.219 nm for the truncated octahedron, which closely matches that of the (111) plane of Pt_3Ni alloy (0.221 nm) (Figure 1d). The cube had a *d* spacing of 0.190 nm, which could be assigned to the (200) plane of Pt_3Ni alloy (0.191 nm) (Figure S2). Both cubes and truncated octahedra had a distance of ∼5 nm between the opposite faces for the particles shown in Figure 1a,c and ∼7 nm for the particles shown in Figure 1b. In addition to the alkane chain length, the reduction rate is critical for controlling both the composition and shape of Pt−Ni alloy nanoparticles. A combination of strong (TBAB) and mild (hexadecanediol) reducing agents was necessary to achieve the proper nucleation and growth rate. When only TBAB was used, irregularly faceted particles were formed (Figure S3).

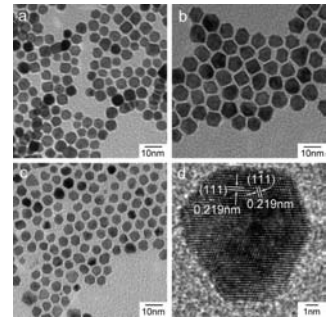

Figure 1. TEM images of Pt_3Ni nanocrystals with truncated octahedron populations of (a) 70%, (b) 90%, and (c) 100%. (d) High-resolution TEM image of a truncated octahedron showing the (111) lattice.

Figure 2 shows a high-angle annular dark-field scanning transmission electron microscopy (HAADF-STEM) image and its corresponding Pt and Ni elemental maps along with a representative energy-dispersive X-ray (EDX) analysis of the 100% *t,o*-Pt_3Ni nanoparticles. Both Pt and Ni were distributed evenly in each nanoparticle (Figure 2a−c; Figure S4 shows an enlarged figure). The Pt/Ni atomic ratio was 76/24, which is close to the composition of Pt_3Ni (Figure 2d). Similar Pt/Ni atomic ratios were observed for the other two *t,o*-Pt_3Ni samples (Figure S5).

The powder X-ray diffraction (PXRD) patterns of these truncated octahedra could all be indexed to (111), (200), (220), and (311) diffractions of a face-centered-cubic (fcc) structure with the peak positions in between those of Pt and Ni metals (Figure 2e). The

[†] University of Rochester.
[‡] General Motors Research and Development.

 10.1021/ja100571h

lattice constant was calculated to be 3.84 Å for the cube-free nanoparticles on the basis of the PXRD data. This value corresponds to a composition around Pt_3Ni calculated according to Vegard's law and assuming $a_{Pt} = 3.923$ Å and $a_{Ni} = 3.524$ Å. The crystalline domain size was measured to be ~6 nm using the full width at half-maximum of the (111) diffraction and the Debye−Scherrer formulation. This value is close to the dimension shown in the TEM images (Figure 1c). The other two types of nanoparticles had similar PXRD patterns, though the 90% *t,o*-Pt_3Ni sample had sharper peaks than the others because of a larger particle size.

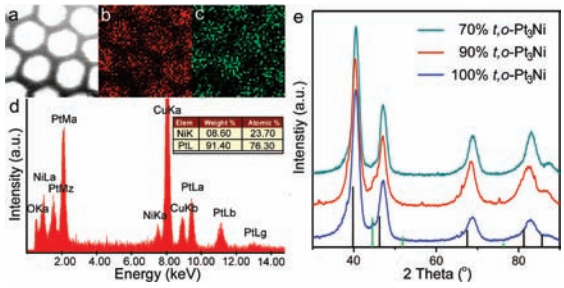

Figure 2. (a) HAADF-STEM image, its corresponding (b) Pt (M line) and (c) Ni (K line) elemental maps, and (d) an EDX spectrum of *t,o*-Pt_3Ni nanoparticles. (e) PXRD patterns of the three Pt_3Ni samples.

These shape-controlled Pt_3Ni nanoparticles were loaded onto a carbon support (Vulcan XC-72) and subsequently treated with butylamine (see the Supporting Information). This mild room-temperature treatment was an important step in the production of active catalysts, as butylamine did not cause any changes in the morphology of the nanoparticles (Figure S6). Figure 3 shows the electrochemical properties of these carbon-supported Pt_3Ni catalysts and a Pt reference catalyst (TKK, 50 wt % Pt, 3 nm diameter on Vulcan carbon; Figure S7). The electrochemical surface areas (ECSAs) for these Pt_3Ni catalysts were found to be 33.8, 53.7, and 62.4 m^2/g_{Pt} for the 70, 90, and 100% *t,o*-Pt_3Ni catalysts, respectively, on the basis of the calculated hydrogen adsorption/desorption charge using cyclic voltammetry (CV) data (Figure 3a and Table S1), assuming 210 $\mu C/cm^2_{Pt}$.[8]

Rotating disk electrode (RDE) polarization curves showed that all three Pt_3Ni catalysts had more positive onset potentials and were more active than Pt (Figure 3b and Table S1). From these polarization curves, we determined the area-specific ORR activities (i_s) to be 850 $\mu A/cm^2_{Pt}$ at 0.9 V for the 100% *t,o*-Pt_3Ni catalyst and 215 $\mu A/cm^2_{Pt}$ for the Pt catalyst, showing an ~4-fold enhancement in ORR kinetics (Figure 3b). In comparison, the area-specific activity reported for vacuum-prepared extended-single-crystal $Pt_3Ni(111)$ was 18 mA/cm^2 at 0.9 V,[2] suggesting that an order-of-magnitude further improvement should be possible.

The corresponding ORR mass activity (i_m) was 0.53 A/mg_{Pt} for the 100% *t,o*-Pt_3Ni catalyst, which is ~4 times higher than that of the standard Pt/C catalyst (0.14 A/mg_{Pt}; Figure 3c)[9] and 1.8 times higher than that of carbon-supported octahedral Pt_3Ni catalysts prepared using $W(CO)_6$ as an additive (0.3 A/mg_{Pt}).[6c]

The area-specific activity for ORR has been observed to increase with a change from the (100) to the (111) Pt_3Ni surface.[2,6c,9] The observed differences in the mass and area-specific ORR activities increased almost proportionally with the increase in the fraction of (111) surface over the entire surface areas of the catalysts, agreeing well with the general trend observed in the single-crystal surface study (Figure 3d; see the Supporting Information for a detailed analysis).

In summary, this work provides an approach to the production of shape- and composition-controlled Pt_3Ni catalysts that have shown as much as 4 times the mass activity of the commercial Pt catalyst and have potential for significantly greater improvements if the facet size and surface treatment can be further optimized.

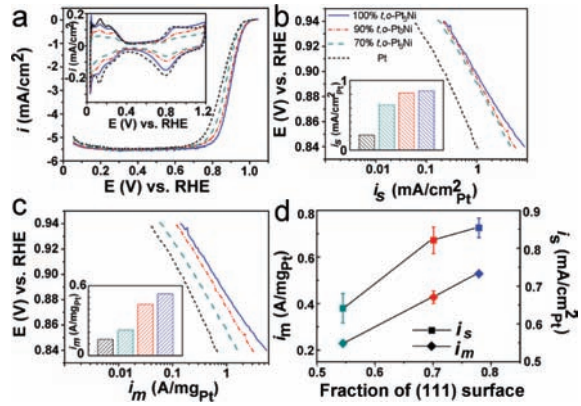

Figure 3. (a) Polarization and (inset) CV curves and (b) area-specific (mA/cm^2_{Pt}) and (c) mass (A/mg_{Pt}) ORR activities for the *t,o*-Pt_3Ni and reference Pt catalysts. (d) Correlations of the area-specific and mass activities with the fraction of (111) surfaces of these Pt_3Ni catalysts. The ORR polarization curves were collected at 1600 rpm.

Acknowledgment. This work was supported in part by NYSERDA (PON 957) and NSF (DMR-0449849). We thank M. F. Mathias for helpful discussions. S.Y. is a visiting student from Xi'an Jiaotong University.

Supporting Information Available: Detailed synthesis and characterization procedures and TEM, XRD, EDX, and electrochemical activity data. This material is available free of charge via the Internet at http://pubs.acs.org.

References

(1) (a) Gasteiger, H. A.; Markovic, N. M. *Science* **2009**, *324*, 48. (b) Gasteiger, H. A.; Kocha, S. S.; Sompalli, B.; Wagner, F. T. *Appl. Catal., B* **2005**, *56*, 9. (c) Peng, Z. M.; Yang, H. *Nano Today* **2009**, *4*, 143. (d) Chen, J. Y.; Lim, B.; Lee, E. P.; Xia, Y. N. *Nano Today* **2009**, *4*, 81. (e) de Bruijn, F. A.; Dam, V. A. T.; Janssen, G. J. M. *Fuel Cells* **2008**, *8*, 3.

(2) Stamenkovic, V. R.; Fowler, B.; Mun, B. S.; Wang, G. F.; Ross, P. N.; Lucas, C. A.; Markovic, N. M. *Science* **2007**, *315*, 493.

(3) Tian, N.; Zhou, Z. Y.; Sun, S. G.; Ding, Y.; Wang, Z. L. *Science* **2007**, *316*, 732.

(4) Mun, B. S.; Watanabe, M.; Rossi, M.; Stamenkovic, V.; Markovic, N. M.; Ross, P. N. *Surf. Rev. Lett.* **2006**, *13*, 697.

(5) Rioux, R. M.; Song, H.; Grass, M.; Habas, S.; Niesz, K.; Hoefelmeyer, J. D.; Yang, P.; Somorjai, G. A. *Top. Catal.* **2006**, *39*, 167.

(6) (a) Lim, B.; Jiang, M. J.; Camargo, P. H. C.; Cho, E. C.; Tao, J.; Lu, X. M.; Zhu, Y. M.; Xia, Y. A. *Science* **2009**, *324*, 1302. (b) Peng, Z. M.; Yang, H. *J. Am. Chem. Soc.* **2009**, *131*, 7542. (c) Zhang, J.; Yang, H.; Fang, J.; Zou, S. *Nano Lett.* **2010**, *10*, 638. (d) Ahrenstorf, K.; Heller, H.; Kornowski, A.; Broekaert, J. A. C.; Weller, H. *Adv. Funct. Mater.* **2008**, *18*, 3850. (e) Maksimuk, S.; Yang, S. C.; Peng, Z. M.; Yang, H. *J. Am. Chem. Soc.* **2007**, *129*, 8684. (f) Koh, S.; Strasser, P. *J. Am. Chem. Soc.* **2007**, *129*, 12624. (g) Habas, S. E.; Lee, H.; Radmilovic, V.; Somorjai, G. A.; Yang, P. *Nat. Mater.* **2007**, *6*, 692. (h) Lee, H. J.; Habas, S. E.; Somorjai, G. A.; Yang, P. D. *J. Am. Chem. Soc.* **2008**, *130*, 5406. (i) Wang, C.; Daimon, H.; Lee, Y.; Kim, J.; Sun, S. *J. Am. Chem. Soc.* **2007**, *129*, 6974. (j) Greeley, J.; Stephens, I. E. L.; Bondarenko, A. S.; Johansson, T. P.; Hansen, H. A.; Jaramillo, T. F.; Rossmeisl, J.; Chorkendorff, I.; Nørskov, J. K. *Nat. Chem.* **2009**, *1*, 552. (k) Ma, Y. G.; Balbuena, P. B. *J. Phys. Chem. C* **2008**, *112*, 14520. (l) Zhang, J.; Sasaki, K.; Sutter, E.; Adzic, R. R. *Science* **2007**, *315*, 220. (m) Chen, S.; Ferreira, P. J.; Sheng, W. C.; Yabuuchi, N.; Allard, L. F.; Shao-Horn, Y. *J. Am. Chem. Soc.* **2008**, *130*, 13818.

(7) (a) Mullen, T. J.; Dameron, A. A.; Saavedra, H. M.; Williams, M. E.; Weiss, P. S. *J. Phys. Chem. C* **2007**, *111*, 6740. (b) Maksimuk, S.; Teng, X.; Yang, H. *J. Phys. Chem. C* **2007**, *111*, 14312.

(8) The saturation hydrogen coverage has been shown to vary for the different crystal faces of Pt alloys (see ref 2); therefore, these surface areas are approximations.

(9) Markovic, N.; Gasteiger, H.; Ross, P. N. *J. Electrochem. Soc.* **1997**, *144*, 1591.

JA100571H